Geophysical Prospecting

EAGE EUROPEAN ASSOCIATION OF GEOSCIENTISTS & ENGINEERS

*Geophysical Prospecting*, 2015, **63**, 1213–1223 doi: 10.1111/1365-2478.12217

# Utilizing spectral decomposition to determine the distribution of injected $CO_2$ at the Snøhvit Field

James C. White[1]*, Gareth A. Williams[1], Sissel Grude[2] and R. Andrew Chadwick[1]

[1]*British Geological Survey, Keyworth, Nottingham, NG12 5GG, U.K., and* [2]*NTNU, S.P. Andersens vei 15A, 7491, Trondheim, Norway*

Received April 2014, revision accepted July 2014

## ABSTRACT

Time-lapse 3D seismic reflection data, covering the $CO_2$ storage operation at the Snøhvit gas field in the Barents Sea, show clear amplitude and time-delay differences following injection. The nature and extent of these changes suggest that increased pore fluid pressure contributes to the observed seismic response, in addition to a saturation effect.

Spectral decomposition using the smoothed pseudo-Wigner–Ville distribution has been used to derive discrete-frequency reflection amplitudes from around the base of the $CO_2$ storage reservoir. These are utilized to determine the lateral variation in peak tuning frequency across the seismic anomaly as this provides a direct proxy for the thickness of the causative feature.

Under the assumption that the lateral and vertical extents of the respective saturation and pressure changes following $CO_2$ injection will be significantly different, discrete spectral amplitudes are used to distinguish between the two effects. A clear spatial separation is observed in the distribution of low- and high-frequency tuning. This is used to discriminate between direct fluid substitution of $CO_2$, as a thin layer, and pressure changes that are distributed across a greater thickness of the storage reservoir. The results reveal a striking correlation with findings derived from pressure and saturation discrimination algorithms based on amplitude versus offset analysis.

**Key words:** Time lapse, Seismic, Monitoring, $CO_2$ storage, Spectral decomposition, Peak frequency shift, Carbon capture and storage.

## INTRODUCTION

Thin layers within a geological succession can enhance or diminish distinct frequencies within a propagating seismic wavelet depending on their temporal thicknesses (Partyka, Grigley, and Lopez 1999). Thin layers of spreading $CO_2$ are expected to generate similar responses in time-lapse seismic data. In this study, we exploit spectral tuning effects in time-lapse 3D seismic data acquired over the $CO_2$ storage operation at the Snøhvit field in the Barents Sea (see Fig. 1a). The thickness of a causative layer can be assessed by analysing discrete Fourier components from the data since reflections from the top and the base will interfere in boosting the spectral amplitudes at certain frequencies. This technique, broadly termed spectral decomposition, has previously enabled authors to enhance the imaging of complex geological structures (Laughlin, Garossino, and Partyka 2003; McArdle and Ackers 2012) and to classify and describe stratigraphic sequences as a function of their spectral response (Partyka *et al.* 1999; Chen *et al.* 2008). The application of this method to layers of $CO_2$ necessitates the extraction of spectral data from short time windows within the seismic trace and provides an additional layer of complexity to the study. The smoothed pseudo-Wigner–Ville distribution (SPWVD) is employed (Williams and Chadwick 2012) since it offers an acceptable compromise between temporal windowing and spectral resolution. This

*E-mail: jame3@bgs.ac.uk

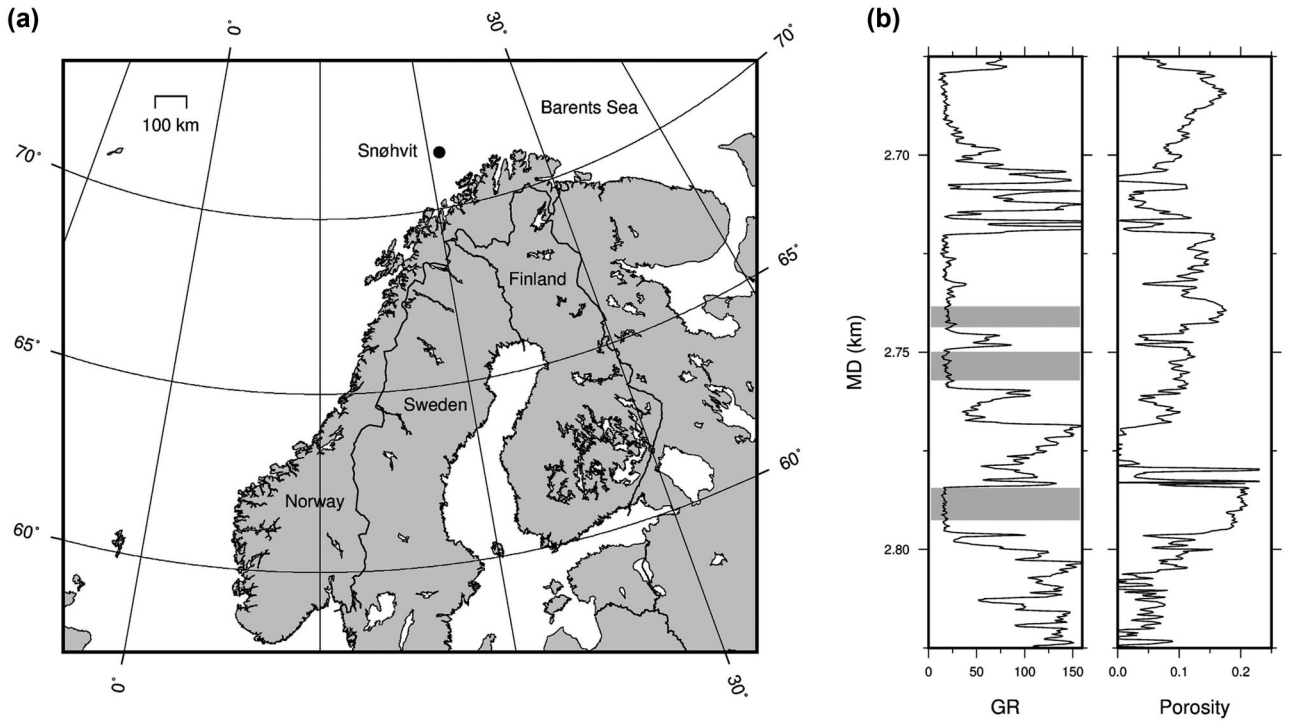


**Figure 1** (a) Location of the Snøhvit $CO_2$ storage operation in the Barents Sea, Norway. (b) Gamma ray and porosity logs from the injection well. The *y*-axis shows measured depth as the well is deviated; the Tubåen Formation is located between 2.68 km and 2.8 km. The grey boxes highlight the injection perforation zones. The reservoir sands show low gamma-ray (GR) and higher porosity.

methodology has previously been used (Williams and Chadwick 2012; White, Williams, and Chadwick 2011; White, Williams, and Chadwick 2013) to analyse the upper $CO_2$ layer at the Sleipner injection site in the Norwegian North Sea.

Analysis of the Snøhvit $CO_2$ injection programme relates to the period prior to the 2009 3D seismic monitoring survey. This followed the injection of ~0.5 million tons of $CO_2$ between April 2008 and August 2009. During this period, the $CO_2$ injection was at the base of the Tubåen Formation, a fluvial-to-tidal sandstone of approximately 100-m thickness, at a depth of 2565–2665 m below sea level. A consequence of injecting $CO_2$ into the faulted, seemingly structurally compartmentalized Tubåen reservoir is the pressuring-up of the pore fluid in the injection fault block (Hansen *et al.* 2011).

Time-lapse seismic data acquired over reservoirs with a limited volume are known to display responses attributable to both pressure and saturation changes (Angelov, Spetzler, and Wapenaar 2004; Landrø 2001). The increase in pore pressure reduces the effective stress in the formation and causes a decrease in the p-wave velocity, which may produce a detectable signal in the seismic difference data.

This study aims to utilize the spectral decomposition technique to define the limits of $CO_2$ saturation changes (where $CO_2$ replaces brine) and then differentiate the pressure-induced seismic signature from that caused by the direct fluid substitution. Previously, pressure–saturation discrimination schemes have relied upon the analysis of amplitude differences and travel-time changes between different vintages (Tura and Lumley 1999; Trani *et al.* 2011; Tatanova and Hatchell 2012). These studies generally build on two earlier papers: Brevik (1999) introduced a methodology to derive pressure and saturation variations through the inversion of travel-time differences, whereas Landrø (1999, 2001) developed a scheme that used the amplitude versus offset (AVO) characteristics of seismic reflections to separate the effects.

Grude *et al.* (2013) have analysed the same seismic data available to this study, acquired over the $CO_2$ storage site at the Snøhvit field, using a modified version of the time-lapse pressure–saturation inversion scheme developed by Landrø (2001). Their analysis aimed to discriminate between pressure and saturation effects, utilizing the different AVO responses of the two processes. Their results are compared with ours, which are derived from spectral decomposition.

 

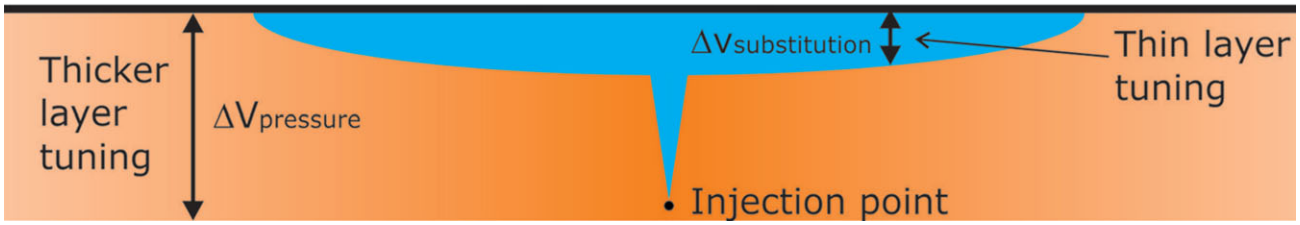


**Figure 2** A simple schematic highlighting the different thicknesses of fluid substitution (blue) and pressure (orange) anomalies. $CO_2$ characteristically spreads as thin layers, but the pressure increase in closed reservoirs spreads more extensively. The different vertical extents will tune different frequencies in the seismic wavelet.

The spectral decomposition methodology requires the acquisition of baseline (pre-injection) and repeat (post-injection) 3D seismic data. The technique relies upon the fact that different layer temporal thicknesses will preferentially tune different frequencies. Assessing the response across a spectral bandwidth equivalent to the source wavelet allows discrete-frequency reflection amplitudes to be derived. These amplitudes are normalized to the spectral content of the band-limited seismic wavelet then the equivalent pre-injection spectral response is removed. This allows the reflectivity developed as a consequence of the injection can be determined as a function of frequency. Ascertaining which spectral component displays the greatest change then gives a measure of the temporal thickness of the layer. The following workflow should provide a method to assess the vertical thickness of the layer generated during $CO_2$ injection.

- Isolate and extract the seismic response from a single layer.
- Derive discrete-frequency reflection amplitude data over the spectral bandwidth.
- Normalize the discrete-frequency reflection amplitude by the seismic wavelet.
- Remove the baseline response from time-lapse data.
- Determine the tuning frequency of the reflection coefficient pair.
- Derive the temporal thickness across the lateral extent of the anomaly.

An important aspect of this study is the further evidence of how an accurate baseline 3D seismic data set is necessary to monitoring subsequent injection with time-lapse surveys.

## SPECTRAL DECOMPOSITION

The emplacement of highly compressible $CO_2$ brings about a reduction in the velocity of the propagating wavefield, and subsequent deeper reflections display a characteristic velocity pushdown in their arrival times. In addition, the $CO_2$ will generate readily observable reflectivity responses on time-lapse seismic difference data, which enable the lateral delineation of injected $CO_2$. However, if the injection reservoir has a limited volume into which the pressure increase caused by injection can dissipate, the pressure anomaly might also create a measurable response on time-lapse seismic data. The hypothesis tested in this study is that the lateral and vertical extents of the respective saturation and pressure changes will be significantly different. As such, it should be possible to discriminate between the two processes. In general terms, injected $CO_2$ characteristically spreads laterally in the reservoir as thin layers (e.g., Chadwick *et al.* 2004), whereas the pressure response is transmitted through the aquifer brine and spreads more widely (vertically and horizontally) through the reservoir. These different vertical extents will each display a characteristic spectral response that can be exploited (Fig. 2). It is noted that changes in pore fluid pressure are likely to be coincident with the fluid substitution close to the injection well and that their effects might be masked by this higher amplitude signal where they overlap.

Both pressure and saturation anomalies will produce a new, or altered, subsurface layer where the reflection from the top and the bottom will differ from the response in the baseline survey. If the layer is suitably thin, the top and base reflections will interfere to produce a tuned wavelet. Spectral tuning of the wavelet occurs at, $f$, such that

$$f = 1/(2T), \tag{1}$$

and at subsequent harmonic modes where

$$f = (n + 1/2)/T, \tag{2}$$

with $T$ being the two-way temporal thickness of the layer, and $n$ being an odd integer. As such, the tuning frequency is a function of the two-way travel-time thickness of the layer (see Fig. 3).

A small analysis window is required to isolate reflections from the individual $CO_2$ layers. Hence, conventional time–frequency analysis techniques suffer from resolution

 

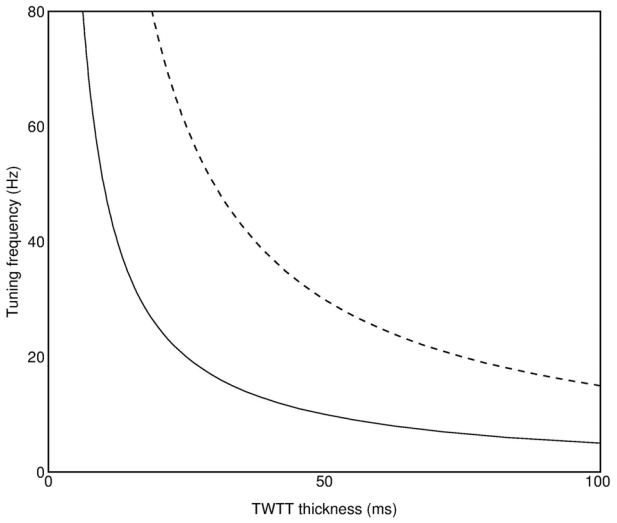


**Figure 3** First spectral peak (tuning frequency) and second tuning harmonic (dashed line) as a function of two-way travel-time thickness.

problems; a narrow analysis window localizes the spectrum in time but provides poor frequency resolution. Isolating the spectral response from a single causative layer in seismic data is non-trivial, and Williams and Chadwick (2012) undertook an assessment of various spectral windowing techniques.

The Wigner – Ville Distribution ($W_{x(t,f)}$) of a function $x$,

$$W_{x(t,f)} = \int_{-\infty}^{+\infty} x\left(t+\frac{\tau}{2}\right) x^*\left(t-\frac{\tau}{2}\right) \mathrm{e}^{-i2\pi f\tau} d\tau \tag{3}$$

is constructed by computing the auto-correlation over all possible lags at each time sample (the local auto-correlation function) and transforming it into Fourier space, where $t$ is the time, the time, $\tau$ is the lag, $f$ is the frequency, and $^*$ represents complex conjugation.

This algorithm is a quadratic function, and consequently, discrete events in a time series produce cross terms in the time–frequency distribution. The cross terms can be reduced by smoothing with an appropriate filter kernel along the time and frequency axes to give the SPWVD,

$$SPWVD_{x(t,f)} = \int_{-\infty}^{+\infty} h(\tau) \int_{-\infty}^{+\infty} g(x-t)\, x\left(t+\frac{\tau}{2}\right) x^* \times \left(t-\frac{\tau}{2}\right) dt\, \mathrm{e}^{-i2\pi f\tau} d\tau \tag{4}$$

where $g(x-t)$ and $h(\tau)$ are the smoothing kernels in time and frequency respectively (Flandrin and Escudie 1984). Williams and Chadwick (2012) established that a suitable tradeoff between temporal windowing and spectral resolution was achieved with the quadratic SPWVD. This algorithm is used in the remainder of this study to extract discrete-frequency spectral amplitudes.

The principle of our method is illustrated by a synthetic seismic example, which models the pore pressure and fluid substitution changes generated during $CO_2$ injection (Fig. 4). Initially, in the baseline case, a Ricker wavelet with a peak frequency of 25 Hz is incident on an arbitrary interface at 400-ms two-way travel time (Fig. 4a). The same source wavelet is then incident on two different thin layers representing distinct time-lapse responses: a 15-m layer where $CO_2$ has replaced brine (Fig. 4b) and a 36-m-thick pore pressure anomaly (Fig. 4c). As such, these seismic traces contain a superposition of two reflections. A noticeable pushdown of the primary reflection is apparent in the time-lapse seismic, a consequence of the velocity reduction following injection. Fig. 4d displays the spectral response from the single reflection in the baseline case. The red lines in Fig. 4e and f show the spectral content of the reflection pairs, from the top and base of the new layer, following fluid substitution and pore pressure changes, respectively. The accompanying blue lines show the same spectra normalized by the baseline response. In practice, at each discrete frequency, the time-lapse spectral amplitude is divided by the pre-injection response; therefore, where no spectral tuning occurs, a value of one is returned. It is clear that the peak spectral energy content has shifted. The peaks define the tuning frequency for the top and base reflections. The normalized spectrum in Fig. 4e has a peak frequency of ~29 Hz. This correctly corresponds to a temporal thickness of 17 ms. The amplitude boost obtained from tuning seen in Fig. 4f is less pronounced. A peak frequency of ~17 Hz is evident, equivalent to the correct temporal thickness of 30 ms. The second peak frequency at 51 Hz corresponds to the second tuning harmonic.

## SNØHVIT TIME-LAPSE SEISMIC DATA

$CO_2$ injected at Snøhvit is separated from natural gas extracted from the overlying gas field. Hydrocarbon gas, which contains ~6% $CO_2$, is piped to shore 150 km away for processing before $CO_2$ is returned by the pipeline. The injection infrastructure sits on the seabed in ~300 m water depth. This study assesses the effects of $CO_2$ injection prior to the 2009 3D seismic monitoring survey that followed the injection of 0.5 Mtons over a 16-month period. Injection was into the Tubåen Formation, a fluvial-to-tidal sandstone deposit of

 

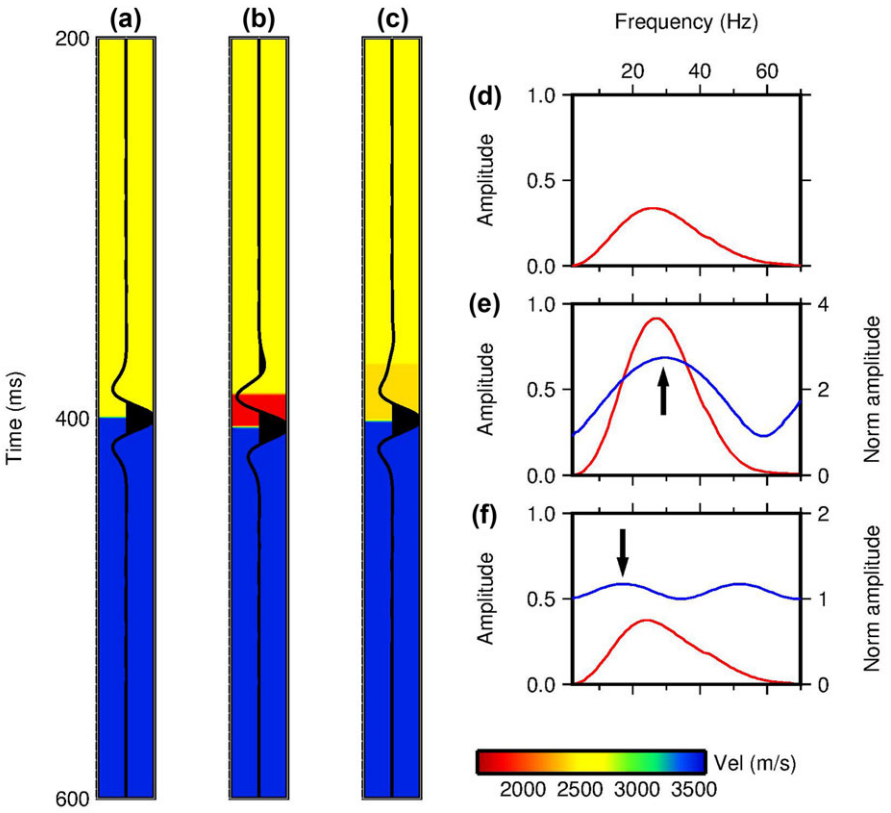


**Figure 4** Synthetic time-lapse seismic response mimicking $CO_2$ injection into a closed reservoir. (a), (b), and (c) display a seismic trace from the baseline, fluid substitution, and pore pressure anomaly examples overlying their respective velocity models. The red lines in (d), (e), and (f) display the spectral amplitude from each example, whereas the blue lines show the baseline normalized time-lapse responses (using right axis) and highlight the change in peak frequency (see arrows) caused by tuning effects.

approximately 100 m thickness, at depth of 2565–2665 m below sea surface (Hansen *et al.* 2011).

The Tubåen Formation is predominantly deltaic sediments with both marine and fluvial influences. Analysis of the injection well log reveals the presence of four or five inter-bedded shale layers, which are likely to hinder vertical flow. The sand units are classed as exceptionally clean (Grude, Landrø, and Osdal 2013). The lowest clean unit, approximately 15 m thick, was believed to be high-porosity and high-permeability channel sand. Gamma ray and porosity logs from the injection well (Fig. 1b) reveal the variable sand quality in the reservoir. Analyses of further exploration wells that penetrate the Tubåen Formation suggest that the distribution of sand and shale is irregular as the correlation of specific bodies is demanding (Maldal and Tappel 2004). As such, the sandstone units are likely to be interconnected over distances shorter than the width of the fault blocks, meaning vertical communication through the Tubåen Formation is likely. $CO_2$ was injected through three perforations in the middle and lower sections of the reservoir.

During injection, the reservoir proved to be more complicated than originally anticipated with significant permeability problems. These have been attributed to quartz cementation, more substantial fluvial channelling than anticipated, and the possibility of faults in the formation hindering flow. Horizontal permeability values range from millidarcies to several darcies, whereas porosity values between 8% and 20% are observed (Hansen *et al.* 2013).

The seismic surveys utilized in this study were collected in 2003 and 2009, both with inlines orientated North–South. A shared lateral extent of 8.25 km x 9.65 km is analysed. Source steering ensured an excellent match of source and receiver locations between the 2003 and 2009 surveys, and repeatability metrics are high (Hansen *et al.* 2011).

Cross-sections from the seismic data are displayed in Fig. 5 and intersect the injection point. The top Tubåen

 

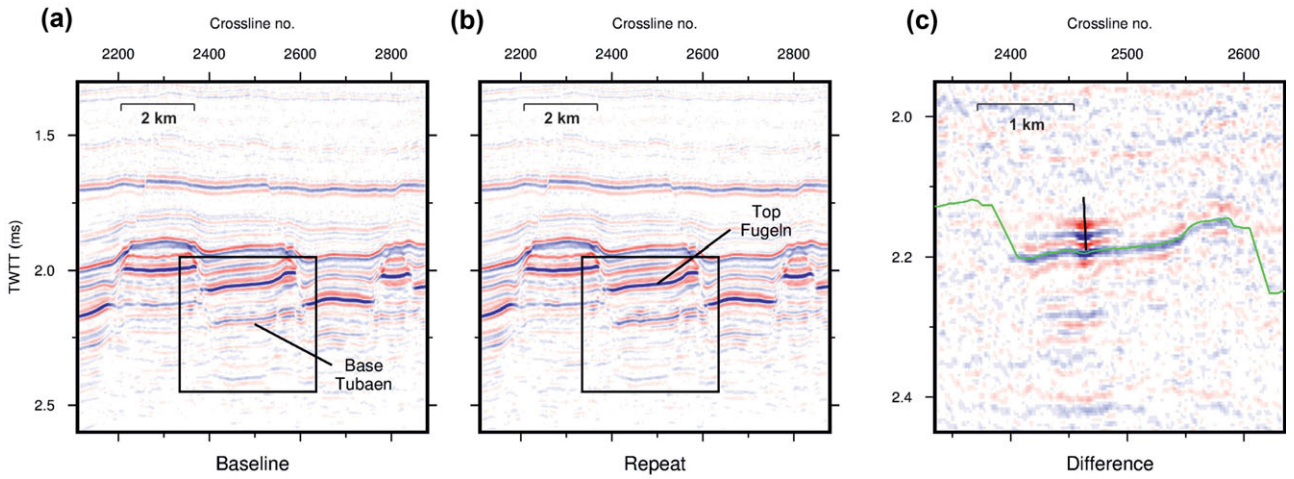


**Figure 5** Seismic sections from (a) the 2003 baseline and (b) the 2009 repeat data cubes. This line crosscuts the injection point and is perpendicular to the orientation of the major regional fault blocks. (c) displays the time-lapse difference data from the region bounded by the black box in (a) and (b). The black line displays the location of the injection well in the storage reservoir. The green line is the picked horizon for the base Tubåen reflection in the 2009 vintage.

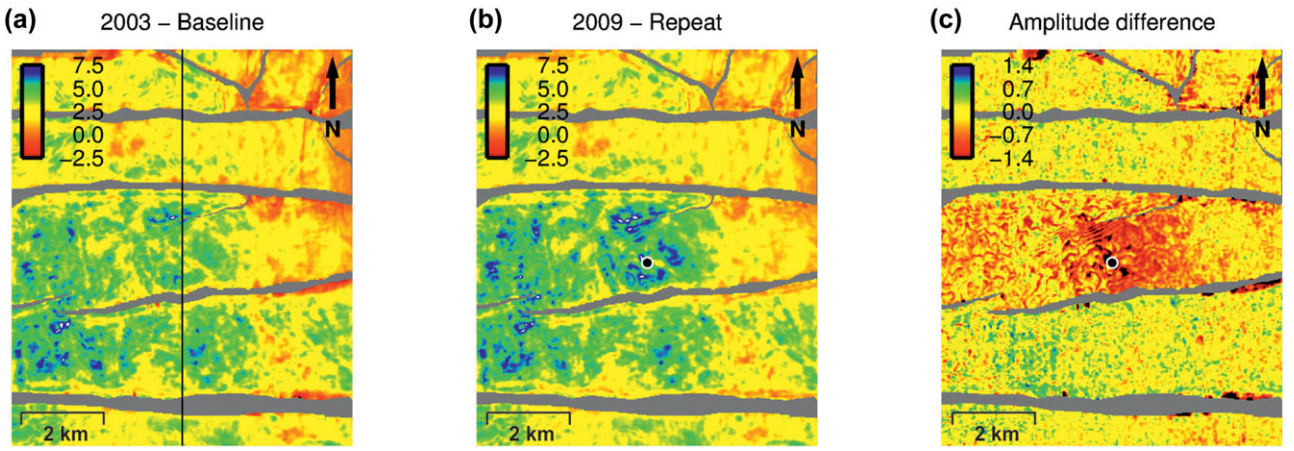


**Figure 6** Reflection amplitudes for the base Tubåen extracted from (a) the baseline and (b) the repeat seismic monitoring surveys at Snøhvit. (c) shows the difference between the grids. The black line highlights the location of the section displayed in Fig. 5. The injection point is shown with a black dot in (b) and (c). Linear grey features correspond to faults that cut the reservoir into separate fault blocks.

reflection is poorly imaged on the seismic with the overlying top Fugeln acting as a regional indicator. The base Tubåen is imaged across the survey area, but reflection amplitudes significantly reduce to the east, possibly as a consequence of an overlying gas accumulation.

Figure 6 shows amplitude plots of the base Tubåen reflection from the 2003 and 2009 surveys, in plan view, alongside a plot of the difference between the two surveys. Facies and porosity changes in the Tubåen Formation are thought to account for variable amplitudes in the baseline survey. The effects of $CO_2$ injection are clear, with the greatest amplitude differences evident close to the injection perforations and on the margins of previous amplitude high values. This suggests that subsurface changes preferentially occur in regions of greater permeability and porosity. Due to the lateral extent of the difference anomaly, it has been postulated that pressuring up of the pore water is responsible for most of the difference signal (Hansen *et al.* 2011; Grude *et al.* 2013). If fluid substitution, that is $CO_2$ replacing brine, were responsible for the entire extent of the anomaly, the $CO_2$ layer could, from volumetric calculations, be at most 1–2 m thick. This layer would be unresolvable with the frequency content of the seismic data and, if detectable, would display a very high tuning frequency. However, with a smaller $CO_2$-saturated zone located close to

 

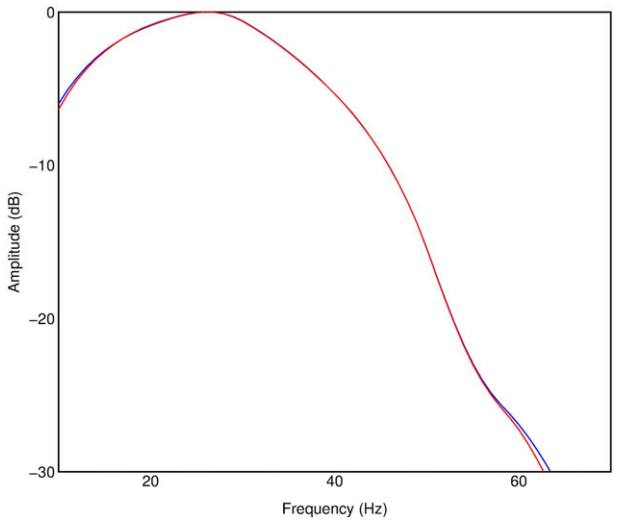


**Figure 7** Maximum reflection amplitude as a function of frequency for the time-lapse data sets from 2003 (blue) and 2009 (red).

the injection point and pooled primarily beneath the deepest intra-Tubåen thin mudstone layer, the spectral content of the data should provide some clues as to its extent.

Conversely, the pressure increase is likely to have a greater vertical extent in the reservoir and will display preferential tuning at lower frequencies. This study postulates that, by assessing the spatial variation in peak tuning frequency around the base Tubåen reflection, it is possible to separate the saturation and pressure effects while acknowledging that the pressure response will be laterally coincident with that from the fluid changes and may generate some signal masking.

## SPECTRAL ANALYSIS OF THE SNØHVIT DATA

Discrete-frequency cubes were generated using the SPWVD from both 3D seismic data sets. The base Tubåen reflection was used to extract discrete-frequency root-mean-square amplitude slices on the seismic pick, and the data were mapped. Noting the band-limited nature of the seismic wavelet, spectral balancing is employed for the Snøhvit time-lapse seismic data. Under the assumption that geologic tuning of every discrete frequency occurs within the seismic volume, the wavelet spectrum can be balanced by equalizing each frequency slice according to its maximum amplitude (see Partyka *et al.* 1999) in the overlying seismic section, windowed between 1.5 seconds and 2.1 seconds. The scaling functions used to balance the data are shown in Fig. 7 and highlight how significant high frequency energy (up to 45 Hz) is still present in the wavefield.

Spectrally balanced single-frequency reflection amplitude plots for the base Tubåen are shown in Fig. 8 from across the usable frequency range. The magnitude of the reflections, across the entire region, shows a steady reduction with increasing frequency. This is likely related to the preferential attenuation of higher frequencies between the balancing window and the storage reservoir. This effect is present in both the baseline and repeat survey data and the baseline normalization procedure should rectify this issue on the 2009 data.

The lower panels in Fig. 8 display the 2009 reflection amplitude data incorporating the baseline normalization procedure and also a clip to remove the very lowest amplitudes. The white dot in the centre of the images marks the injection point. The anomaly surrounds the injection point with no significant difference signal in adjacent fault blocks. The faults cutting the reservoir are shown to be sealing and restricting the effects of injection to the injection block. The outline of the anomaly at the lowest frequency (10 Hz) is comparable with the extent of the feature in the seismic amplitude difference data (Fig. 6). This suggests that most of the difference signal is generated by a layer with a significant temporal thickness. An insufficient amount of $CO_2$ has been injected for direct fluid substitution to cause this response, even at low levels of saturation. This supports the hypothesis that a pore pressure increase, over a greater vertical extent, is responsible for the majority of the difference anomaly. Maldal and Tappel (2004) suggest the individual sand units that make up the Tubåen are in communication, meaning a pressure anomaly over this vertical extent is feasible.

A pressure feature that reaches into the middle and upper Tubåen Formation, with a thickness of 50 m or more, would generate a peak tuning frequency response below 25 Hz. This spectral cut-off is determined using equation 1 and an average p-wave velocity for the Tubåen Formation of 4250 $ms^{-1}$ (Grude *et al.* 2013). The baseline normalized difference plots, in the lower panels of Fig. 8, show a reduction in the lateral extent of the difference amplitude anomaly as frequency increases so the amplitude difference at 10 Hz is interpreted to show that the footprint of the pore pressure change.

The deepest and cleanest sandstone unit within the Tubåen has a thickness of ~15 m (Fig. 1b), and well logs indicate a pre-injection p-wave velocity of ~4100 $ms^{-1}$. Approximately 80% of the injected $CO_2$ is estimated to have pooled in this layer, close to the injection well (Hansen *et al.* 2011; Grude *et al.* 2013). $CO_2$ saturation levels between 0.55

 

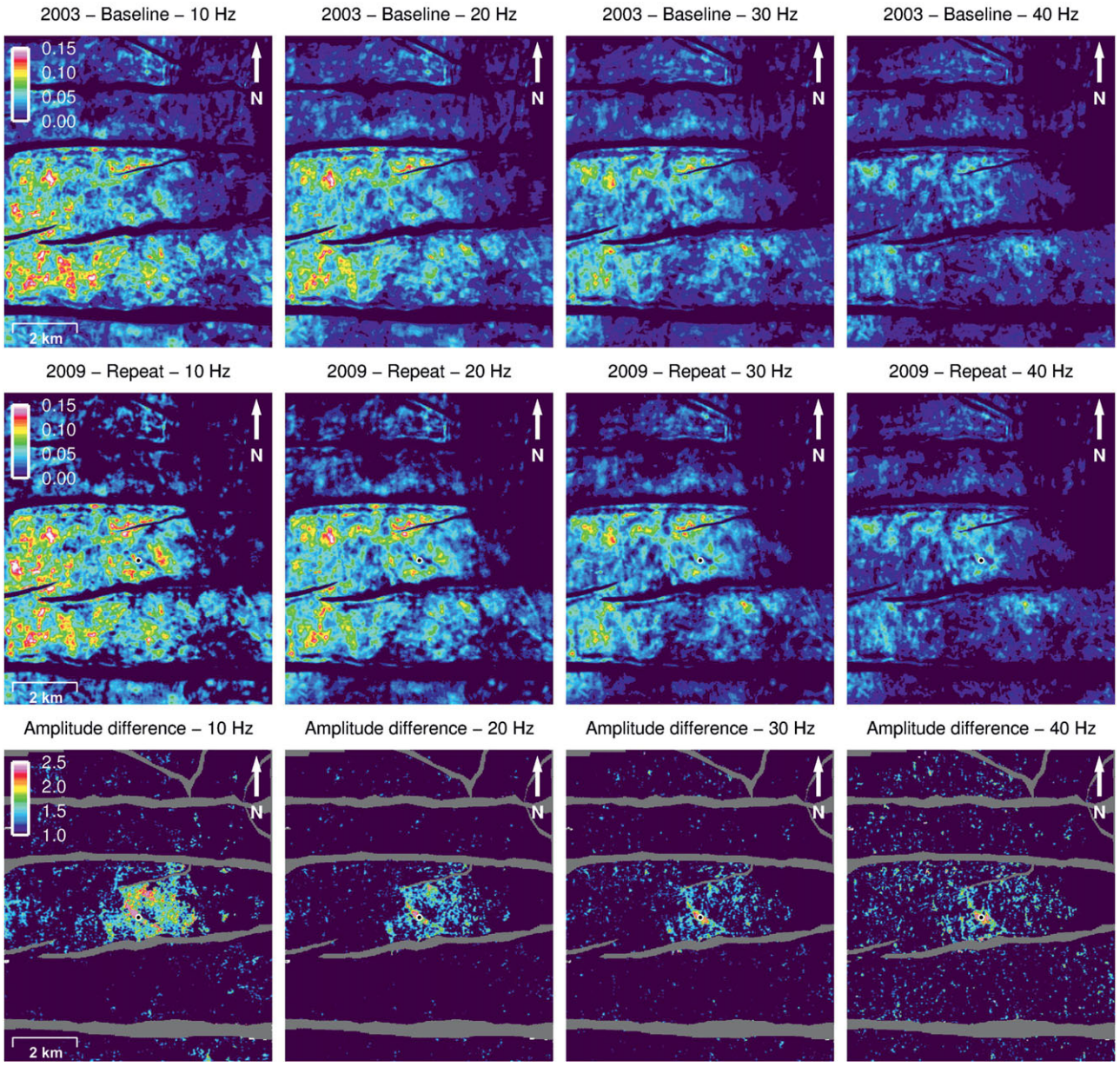


**Figure 8** Frequency normalized reflection amplitude plots for discrete-frequency slices extracted from the baseline (top panels) and repeat (middle panels) surveys. The lower panels display amplitude normalized difference plots for discrete-frequency slices from the repeat survey. The injection point is shown with a black dot. Linear grey features correspond to faults that cut the reservoir into separate fault blocks.

and 0.80 would generate a p-wave velocity drop of the order of 10%. Accounting for this thicknesses and velocity and using equation 1, a peak tuning frequency of 50–60 Hz would be expected. The Snøhvit seismic wavelet might not contain sufficient spectral bandwidth to properly image with the first tuning peak, but it is known that the discrete-frequency amplitudes from a thin layer rapidly increase as the frequency approaches the tuning frequency. This opportune result means that frequencies approaching the tuning value will display increased amplitudes and can be used to constrain the extent of the causitive anomaly. Data above 45 Hz become prohibitively noisy, but the trend clearly illustrated at 30 Hz and 40 Hz (Fig. 8) is likely to be continued.

A clear NW–SE stratigraphical feature is visible across the injection point and is seen right through the frequency range, suggesting that it is a response caused by direct $CO_2$

 

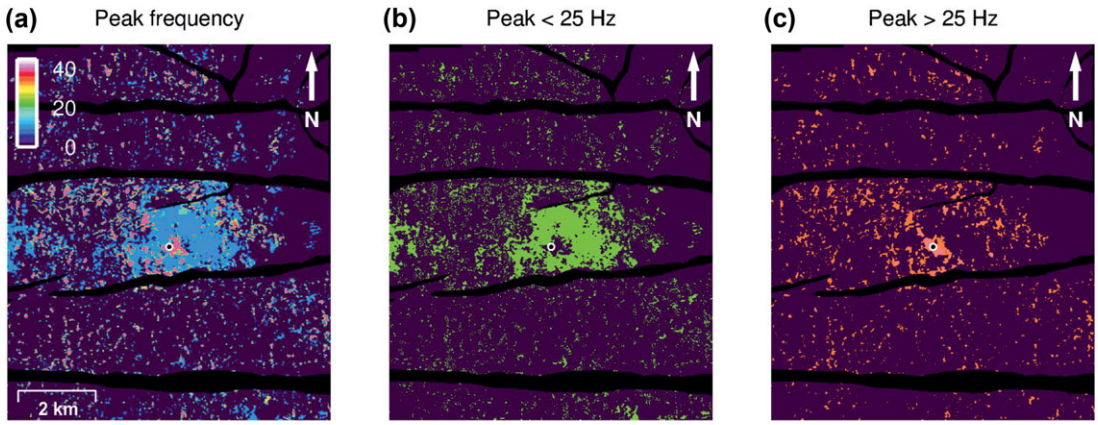


**Figure 9** (a) Frequency displaying the greatest change in amplitude between baseline and repeat 3D seismic surveys. (b) and (c) partition the data either side of a 25 Hz cut-off to separate the contributions from pressure and saturation changes. The injection point is shown with a black dot.

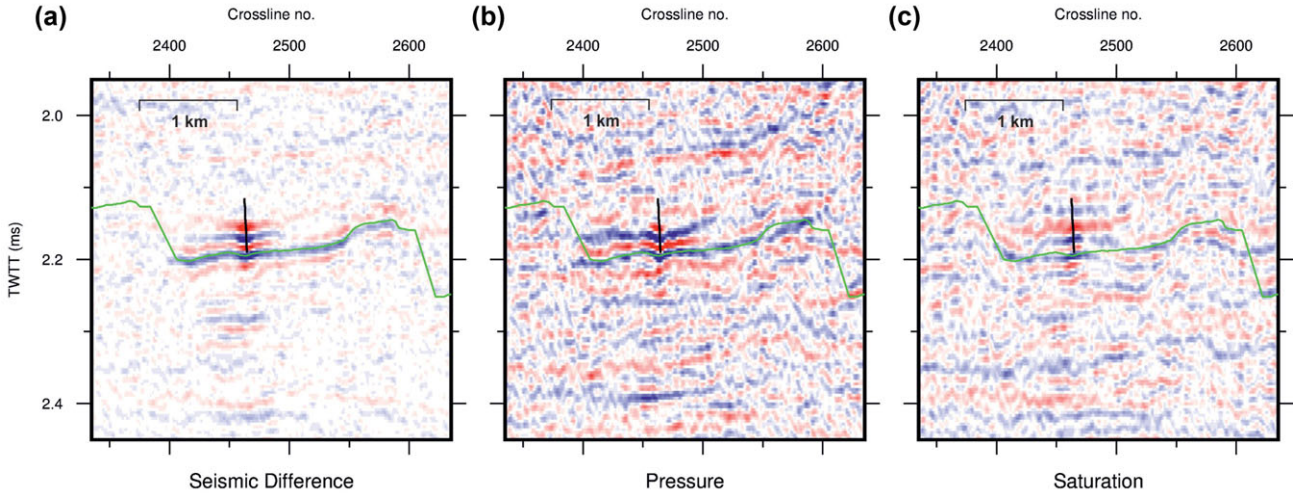


**Figure 10** (a) The time-lapse difference data from the region bounded by the black box in Fig 3. The green line highlights the base Tubåen pick from the 2009 repeat seismic data set. (b) and (c) show the inverted 3D pressure and saturation data for the same region derived by Grude *et al.* (2013). The seismic line crosscuts the injection point and is perpendicular to the orientation of the major regional fault blocks. The black line displays the location of the injection well in the storage reservoir.

substitution. This indicates a higher permeability channel cross-cutting the fault block.

Working under the hypothesis that the pressure signature extends into the middle and upper regions of the reservoir, it is proposed that responses at frequencies above 25 Hz are likely to be derived primarily from $CO_2$ saturation changes. In order to separate the pressure and saturation effects, a spatial analysis to determine the frequency displaying the largest change in amplitude relative to the baseline was performed (Fig. 9a). Where the greatest change is below 25 Hz, it is suggested that a pore pressure increase produces the seismic anomaly. Conversely, where the greatest change occurs at over 25 Hz, the effect is likely due to fluid substitution. Figure 9b and c highlights this separation and justifies the hypotheses that the free $CO_2$ remains close to the injection site.

## DISCUSSION

The separation of pressure and saturation contributions to the seismic response at Snøhvit has been considered previously. Hansen *et al.* (2011) used AVO analysis, noting that pressure changes would primarily be seen on the near offset seismic data, to create a partition of pressure and saturation effects

 

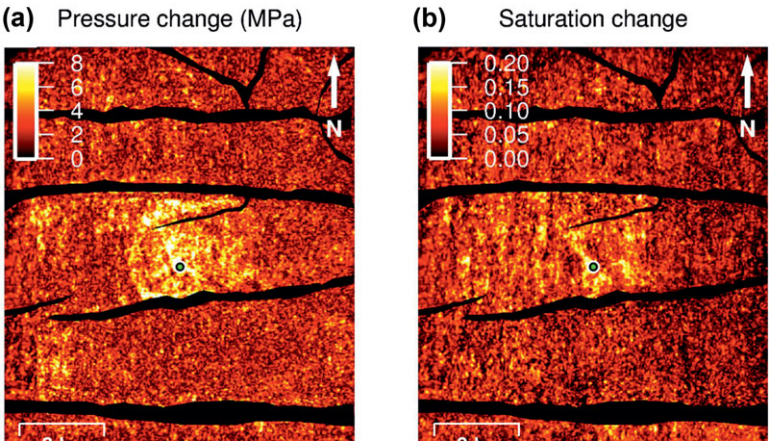


**Figure 11** The inverted pressure and saturation changes around the base Tubåen reflection derived by Grude *et al.* (2013) from reflected seismic amplitudes in near- and far-offset stacks using the methodology described in Landrø (2001). The injection point is shown with a white dot.

from near, middle, and far offset stacks. Their analysis yields a similar result to that presented in Fig. 9.

Grude *et al.* (2013) developed this idea further and used advanced AVO characteristics and time-lapse pressure and saturation discrimination algorithms (Landrø 2001) to split the pressure and saturation components. The inverted pressure and saturation cubes from their analysis (Fig. 10) show the calculated changes along a section through the injection point (same section as Fig. 5). Their results suggest a patchy fluid mixing model with maximum $CO_2$ saturations between 0.15 and 0.5 in the near-well area. The pressure contribution to the base Tubåen reflection is seen to cover a significant proportion of the fault block while the saturation response is localized around the injection point. Grude *et al.* (2013) state that their analysis suggests that the pressure effect dominates the time-lapse seismic difference signal away from the near-well bore area. They calculate a pressure increase of up to 15 MPa (150 bar) close to the injection well and a continuous presure build up of 5 MPa (50 bar) that terminates against the edges of the fault block. These values correspond reasonably well with the bottom hole pressure (BHP) changes recorded in the injection well (Grude *et al.* 2013). Unfortunately the down hole pressure gauge is situated approximately 800 m above the reservoir so BHP values are estimated. Over the course of the injection period a maximum pressure increase of 10 MPa (100 bar) is calculated with a 6 MPa (60 bar) increase estimated at the time of the monitoring survey.

Time slices from the inverted pressure and saturation cubes derived by Grude *et al.* (2013) at the base Tubåen reflection (Fig. 11) reveal a striking correlation with results from the spectral analysis (Fig. 9). In both cases, the derived pore pressure increase was confined to the injection fault block with the associated reduction in effective stress exhibiting a significantly larger footprint than the fluid substitution change. The pressure anomalies have a similar footprint and shape. Fluid substitution occurs at similar locations and is confined to the near-well region. An NW–SE channel around the injection site is defined in both responses and appears to act as a high-permeability pathway for both $CO_2$ and pressure propagation.

## CONCLUSIONS

Spectral decomposition has been used to discriminate between direct fluid substitution and pressure changes in the Tubåen storage reservoir at Snøhvit. A clear spatial separation, on the base Tubåen reflection, is seen between low- and high-frequency tuning. This partitioning has been used to define the lateral extents of the two causative mechanisms. The results show agreement with previous attempts to differentiate between $CO_2$ saturation changes and pressure increases in the Tubåen Formation using different methods (Hansen *et al.* 2011; Grude *et al.* 2013).

The spectral decomposition methodology presented in this paper has been utilized on seismic data covering the $CO_2$ storage operation at Snøhvit. However, it is simply the addition of a contrasting fluid that generates the time-lapse response, which is investigated in this study. As such, the scheme could be used to investigate other scenarios where there is a change in the acoustic impedance properties of the subsurface over a limited vertical extent.

## ACKNOWLEDGEMENTS

Henry Herrera, an anonymous reviewer and the associate editor are thanked for their constructive comments that

 

improved the quality of this manuscript. The authors would like to thank Statoil and their partners for permission to use their data. This publication has been produced with support from the BIGCCS Centre, performed under the Norwegian research programme Centres for Environment-friendly Energy Research (FME). This paper is published with the permission of the Executive Director, British Geological Survey (NERC).

## REFERENCES

Angelov P., Spetzler J. and Wapenaar K. 2004. Pore pressure and water saturation variations: modification of Landrø's AVO approach. SEG technical program, Extended Abstracts, 2279–2282.

Brevik I. 1999. Rock model based inversion of saturation and pressure changes using seismic attenuation. SEG technical program, Extended Abstracts, 1044–1047.

Chadwick R.A., Arts R., Eiken O., Kirby G., Lindeberg E. and Zweigel P. 2004. 4D seismic imaging of an injected $CO_2$ bubble at the Sleipner Field, central North Sea. In: *3-D Seismic technology: Application to the Exploration of Sedimentary Basins*. (eds R.J. Davies, J.A. Cartwright, S.A. Stewart, M. Lappin, and J.R. Underhill). Geological Society, London. Memoir **29**, 305–314.

Chen G., Matteucci G., Fahmy B. and Finn C. 2008. Spectral-decomposition response to reservoir fluids from a deepwater West Africa reservoir. *Geophysics* **73**(6), C23–30.

Flandrin P. and Escudie B. 1984. An interpretation of the Pseudo Wigner-Ville distribution. *Signal Processing* **6**(1), 27–36.

Grude S., Landrø M. and Osdal B. 2013. Time-lapse pressure-saturation discrimination for $CO_2$ storage at the Snøhvit field. *International Journal of Greenhouse Gas Control* **19**, 369–378.

Hansen O., Eiken O., Ostmo S. and Inge Johansen R. 2011. Monitoring $CO_2$ injection into a fluvial brine-filled sandstone formation at the Snøhvit field, Barents Sea. SEG annual meeting, San Antonio, USA.

Hansen O., Gilding D., Nazarian B., Osdal B., Ringrose P., Kristoffersen J.-B., *et al*. 2013. Snøhvit: The history of injecting and storing 1 Mt $CO_2$ in the fluvial Tubåen Fm. *Energy Procedia* **37**, 3565–3573.

Landrø M. 1999. Discrimination between pressure and fluid saturation changes from time-lapse seismic data. SEG technical program, Extended Abstracts, 1651–1654.

Landrø M. 2001. Discrimination between pressure and fluid saturation changes from time-lapse seismic data. *Geophysics* **66**, 836–844.

Laughlin K., Garossino P. and Partyka G. 2003. Spectral decomposition for seismic stratigraphic patterns. *Search and Discovery*, article 40096, 4pp.

Maldal T. and Tappel I.M. 2004. $CO_2$ underground storage for Snøhvit gas field development. *Energy* **29**, 1403–1411.

McArdle N.J. and Ackers M.A. 2012. Understanding seismic thin-bed responses using frequency decomposition and RGB blending. *First Break* **30**, 57–65.

Partyka G., Grigley J. and Lopez J. 1999. Interpretational applications of spectral decomposition in reservoir characterization. *The Leading Edge* **18**, 353–360.

Tatanova M. and Hatchell P. 2012. Time-lapse AVO on deepwater OBN seismic at the Mars field. SEG technical program, Extended Abstracts, 1–5.

Trani M., Arts R., Leeuwenburgh O. and Brouwer J. 2011. Estimation of changes in saturation and pressure from 4D seismic AVO and time-shift analysis. *Geophysics* **76**, C1–C17.

Tura A. and Lumley D.E. 1999. Estimating pressure and saturation changes in time-lapse AVO data. SEG technical program, Extended Abstracts, 1655–1658.

Williams G. and Chadwick A. 2012, Quantitative seismic analysis of a thin layer of $CO_2$ in the Sleipner injection plume. *Geophysics* **77**(6), R245–R256.

White J.C., Williams G. and Chadwick A. 2011. Estimating seismic velocity and thickness of a $CO_2$ layer in the Sleipner plume. *Geophysical Research Abstracts* **13**, EGU2011–3296.

White J.C., Williams G.A. and Chadwick R.A. 2013. Thin layer detectability in a growing CO2 plume: testing the limits of time-lapse seismic resolution. *Energy Procedia* **37**, 4356–4365.